A time-accurate finite element algorithm for incompressible flow problems

M.T. Manzari
Department of Mechanical Engineering, Sharif University of Technology, Tehran, Iran

Received September 2001
Revised March 2002
Accepted August 2002

Keywords *Incompressible flow, Finite elements, Mesh*

Abstract *A finite element solution procedure is presented for the simulation of transient incompressible fluid flows using triangular meshes. The algorithm is based on the artificial compressibility technique in connection with a dual time-stepping approach. A second-order discretization is employed to achieve the required accuracy in real-time while an explicit multistage Runge-Kutta scheme is used to march in the pseudo-time domain. A standard Galerkin finite element method, stabilized by using an artificial dissipation technique, is used for the spatial discretization. The performance of the proposed algorithm is demonstrated by solving a set of internal and external problems including flows with purely transient and periodic behavior.*

Introduction

The study of transient incompressible fluid flow is of prime interest in many engineering applications. The flow characteristic is typically in the form of either a transition from an initial condition to a steady-state or a harmonic response to a cyclic loading. Also, in certain flow regimes such as von Kármán vortex street repeated flow patterns, which are of practical importance, are observed. In particular, the accuracy of the flow simulation in time can be a key issue in some practical problems as various significant modes and regimes might be experienced by the flow during an industrial process. The flow of a fluid with a free surface is a good example with numerous applications in manufacturing. The mould filling in a metal casting process and the injection moulding of polymers are the only two examples of such manufacturing processes (Lewis and Ravindran, 2000). Moreover, the simulation of the unsteady flows has been recently used as a tool for the active control and drag optimization in hydrodynamic design (He *et al.*, 2000).

One of the most successful approaches in the study of incompressible fluid flow is based on the artificial compressibility (AC) concept introduced by Chorin (1967). In this approach, the pressure and velocity fields are coupled by adding a pseudo-time derivative of the pressure to the conservation of mass equation. As a result, the speed of sound waves are reduced from infinity to a finite value and the modified system becomes much better conditioned for a numerical solution. The AC method was first thought to be accurate only for the steady-state problems, however, it has been shown that the method can be equally successful to solve the unsteady flow problems (Merkle and Athavale,

International Journal of Numerical Methods for Heat & Fluid Flow
Vol. 13 No. 2, 2003
pp. 158-177

0961-5539
DOI 10.1108/09615530310459324

1987; Rogers and Kwak, 1989; Soh and Goodrich, 1988). Various types of the upwind (Soh and Goodrich, 1988) and artificial dissipation (AD) schemes have been used in conjunction with AC to provide stable numerical methods. In this work, an AD method by Jameson *et al.* (1981) is adopted due to its simplicity and computational efficiency.

In recent years, significant increase in the computing speed and power has facilitated the study of unsteady flows in complex geometries. Several numerical schemes have been developed for solving incompressible flows in a wide range of flow regimes. These include schemes based on the finite difference (FDM), finite volume (FVM) and finite element (FEM) methods which have been the most popular methods among the CFD practitioners. In the last two decades, a number of FEMs (Brooks and Hughes, 1982; Lewis and Ravindran, 2000; Massarotti *et al.*, 1998) have also been developed and have gained significant popularity due to their sound mathematical bases and ability to handle complex physics. For an extensive discussion on the FEMs, the interested reader can refer the book by Gresho and Sani (2000). Recently, a new approach called the *Edge-based* finite element has attracted the attention of researchers (Manzari *et al.*, 1998; Morgan and Peraire, 1998; Peraire *et al.,* 1993, 1994). This technique attempts to use the capabilities of both the FEM and FVM. The edge-based approach is adopted in this paper.

Also, various numerical techniques such as preconditioning, multigrid (Dailey and Pletcher, 1996; Gatiganti *et al.*, 1998) and parallel processing (Manzari *et al.*, 1998; Wasfy *et al.*, 1998) have been employed to accelerate the solution convergence and reduce the prohibitive CPU time and the memory requirement. Among these different methods, however, those with the least computational complexity and iterative nature are the most favorable as they are more compatible with the new generation of the supercomputers with multiple parallel processors. It is, therefore, the main aim of this paper to devise and examine an accurate and robust yet inexpensive method suitable for such computers.

This work presents an extension of the previous work of the author Manzari (1999) to a time-accurate method for solving unsteady incompressible flow problems. In this paper, first the governing equations for the simulation of a transient incompressible viscous flow are presented and the associated initial and boundary conditions are described. Then, the edge-based finite element procedure used for the spatial discretizations is briefly discussed. The temporal discretization and the use of the dual-time approach is elaborated. Finally, the performance of the proposed method is demonstrated by solving a number of test cases including both external and internal flows. In the case of external flow, first the growth of a re-circulation zone in the wake of a cylinder is studied and then a von Kármán vortex shedding generated behind a cylinder is simulated. The internal flow test cases involve an impulsively started lid driven cavity and a cavity flow with an oscillating lid.

Governing equations

A complete set of equations for unsteady flow of an incompressible fluid consists of equations for conservation of mass and momentum and are known as the Navier-Stokes equations. Due to the lack of a time dependent term in the continuity equation, the pressure and velocity are implicitly coupled through a divergence-free constraint on the velocity. For this reason, the time integration of the incompressible flow equations is not a straight-forward problem and the numerical solution of these equations needs a special treatment. Chorin (1967) remedied the problem by introducing a pseudo-temporal pressure term in the continuity equation. The role of this term is to introduce some kind of AC to the system and make it hyperbolic. As a result, the modified system of equations represents the original form only when a steady-state condition in pseudo-time is reached. It is, however, interesting to note that by adding similar pseudo-time terms to the momentum equations, the system of equations can be modified further to represent the original time-accurate system. This final form is accurate in time as long as the steady-state condition in pseudo-time has reached so that the pseudo-time derivatives vanish. Assuming an isothermal Newtonian fluid, the governing system of equations in a Cartesian coordinate system Ox_1x_2 can be written in the non-dimensional conservation form as

$$\frac{\partial \mathbf{U}}{\partial \tau} + \mathbf{I}^M \frac{\partial \mathbf{U}}{\partial t} + \frac{\partial \mathbf{F}^j}{\partial x_j} = \frac{\partial \mathbf{G}^j}{\partial x_j}, \quad j = 1, 2 \tag{1}$$

where the summation convention is used and

$$\mathbf{U} = \begin{bmatrix} p \\ u_1 \\ u_2 \end{bmatrix} \quad \mathbf{F}^j = \begin{bmatrix} \beta^2 u_j \\ u_1 u_j + p\delta_{1j} \\ u_2 u_j + p\delta_{2j} \end{bmatrix} \quad \mathbf{G}^j = \begin{bmatrix} 0 \\ \tau_{1j} \\ \tau_{2j} \end{bmatrix} \quad \mathbf{I}^M = \begin{bmatrix} 0 & 0 & 0 \\ 0 & 1 & 0 \\ 0 & 0 & 1 \end{bmatrix} \tag{2}$$

In these equations, t denotes the real-time, τ is the pseudo-time, u_i is the velocity in direction x_i, p is the pressure, β^2 is an AC parameter and δ_{ij} is the Kronecker delta. The Reynolds number is defined as

$$\mathrm{Re} \equiv \frac{\rho^* U^* L^*}{\mu_0^*}, \tag{3}$$

where L^* and U^* are the characteristic length and velocity used for non-dimensionalization and μ_0^* is a reference molecular dynamic viscosity. Also, the tensor of viscous stresses τ_{ij} is defined as

$$\tau_{ij} = \frac{\mu}{\mathrm{Re}} \left(\frac{\partial u_i}{\partial x_j} + \frac{\partial u_j}{\partial x_i} \right) \tag{4}$$

The non-dimensional quantities are related to their dimensional counterparts (indicated here by superscript *) via the following relations

$$t = \frac{t^* U^*}{L^*} \quad u_i = \frac{u_i^*}{U^*} \quad p = \frac{p^*}{\rho^* U^{*2}} \quad \mu = \frac{\mu^*}{\mu_0^*} \tag{5}$$

The addition of AC changes the behavior of the inviscid form of the governing equations from parabolic to hyperbolic. In other words, the speed of sound is reduced from infinity to $c = \sqrt{V^2 + \beta^2}$ where V is the local speed of the flow. The AC parameter is, therefore, determined so as to accelerate the convergence to the steady-state solution in pseudo-time. This is discussed later when the time integration scheme is described.

Initial and boundary conditions

A complete mathematical description of the above initial-boundary value problem requires an appropriate set of initial and boundary conditions. Let us consider a computational domain, Ω, which is bounded by a closed boundary, Γ, with unit outward normal vector $\mathbf{n} = (n_1, n_2)$. Two types of problems are considered here: external and internal flows. For external flows, the free-stream values are imposed everywhere in Ω as initial conditions. For internal flows the initial condition depending on the problem specification is either a zero velocity field with a uniform pressure distribution or a solution previously obtained from a steady-state computation.

For an external flow, only flow velocities are imposed at the inflow boundary and the pressure field is computed. At the outflow boundary, however, the pressure field is set to zero and the velocity field is computed. These boundary conditions are accurate when the outflow boundary is placed in a fairly far distance from the body.

At a wall boundary, the no slip condition $u_i = 0$ is imposed except if it is an inviscid wall where a slip condition is imposed for the velocity field by cancelling the normal component of the velocity vector.

Solution algorithm

Spatial discretization

To solve the initial-boundary value problem (1) and (2) using the FEM a weak variational form must be used. This weak form can be written as: find $\mathbf{U}$ such that

$$\int_\Omega \left(\frac{\partial \mathbf{U}}{\partial \tau} + \mathbf{I}^M \frac{\partial \mathbf{U}}{\partial t} \right) W \, \mathrm{d}\Omega = \int_\Omega \mathbf{F}^j \frac{\partial W}{\partial x_j} \, \mathrm{d}\Omega - \int_\Gamma \bar{\mathbf{F}}^j n_j W \, \mathrm{d}\Gamma - \int_\Omega \mathbf{G}^j \frac{\partial W}{\partial x_j} \, \mathrm{d}\Omega + \int_\Gamma \bar{\mathbf{G}}^j n_j W \, \mathrm{d}\Gamma \tag{6}$$

for all suitable weighing functions, W, and for all $t > 0$. Note that from the spatial discretization point of view there is no difference between τ and t. In this expression, an overbar represents a prescribed normal boundary flux.

The two-dimensional computational domain Ω is then discretized using triangular elements, with nodes numbered $1, \ldots, P$ located at the element vertices. Inside each element, a piecewise linear approximate solution is assumed in the form

$$\mathbf{U} \approx \mathbf{U}^{(P)} = \mathbf{U}_J(t) N_J(\mathbf{x}) \quad J = 1, \ldots, P \tag{7}$$

where N_J represents the linear finite element shape function associated with node J and $\mathbf{U}_J$ is the approximated value of the unknown at node J. A Galerkin approximate solution is produced using the variational formulation of the problem in the form: find $\mathbf{U}^{(P)}$ such that

$$\int_\Omega \left(\frac{\partial \mathbf{U}^{(P)}}{\partial \tau} + \mathbf{I}^M \frac{\partial \mathbf{U}^{(P)}}{\partial t} \right) N_I \, \mathrm{d}\Omega = \int_\Omega \mathbf{F}^{j(P)} \frac{\partial N_I}{\partial x_j} \, \mathrm{d}\Omega - \int_\Gamma \bar{\mathbf{F}}^{j(P)} n_j N_I \, \mathrm{d}\Gamma - \int_\Omega \mathbf{G}^{j(P)} \frac{\partial N_I}{\partial x_j} \, \mathrm{d}\Omega + \int_\Gamma \bar{\mathbf{G}}^{j(P)} n_j N_I \, \mathrm{d}\Gamma \tag{8}$$

for $I = 1, 2, \ldots, P$ and for all $t > t_0$. An efficient way of computing the integrals in this Galerkin statement is to use an edge-based data structure as suggested by Peraire *et al.* (1993). The final form of the finite element formulation becomes

$$\left[\mathbf{M} \left(\frac{\partial \mathbf{U}}{\partial \tau} + \mathbf{I}^M \frac{\partial \mathbf{U}}{\partial t} \right) \right]_I = -\sum_{s=1}^{m_I} \frac{C^j_{II_s}}{2} \left\{ (\mathbf{F}^j_I + \mathbf{F}^j_{I_s}) - (\mathbf{G}^j_I + \mathbf{G}^j_{I_s}) \right\} + \left\langle \sum_{f=1}^{2} D_f \{ (4\bar{\mathbf{F}}^n_I + 2\bar{\mathbf{F}}^n_{J_f} + \mathbf{F}^n_I - \mathbf{F}^n_{J_f}) - (4\bar{\mathbf{G}}^n_I + 2\bar{\mathbf{G}}^n_{J_f} + \mathbf{G}^n_I - \mathbf{G}^n_{J_f}) \} \right\rangle_I \tag{9}$$

where s represents the edge connecting node I to I_s, and J_1 and J_2 are the boundary nodes which are connected to the boundary node I. Note that the terms $\langle \cdot \rangle_I$ are only non-zero when node I is a boundary node. The weights $C^j_{II_s}$ and D_f are computed according to

$$C^j_{II_s} = -\sum_{E \in II_s} \frac{2\Omega_E}{3} \left[\frac{\partial N_I}{\partial x_j} \right]_E + \left\langle \sum_{f \in II_s} \frac{\Gamma_f}{6} n_j \right\rangle \quad D_f = -\frac{\Gamma_f}{12} \tag{10}$$

where Ω_E is the surface area of the element E and n_j is the component in the x_j direction of the unit normal to the boundary edge f, of length Γ_f, which connects

the nodes I and J_f. An advantage of this edge data structure is that it leads to the savings in both CPU and memory requirements, especially when three-dimensional simulations are attempted (Peraire *et al.*, 1993). The consistent finite element mass matrix $\mathbf{M}$ in equation (9) is replaced by the diagonal lumped mass matrix $\mathbf{M}_\mathrm{L}$. This approximation makes the computational process much simpler and less expensive without the negative effects on the accuracy for a range of problems solved in this paper.

The nodal values of the gradients of $\mathbf{U}$, which are required before the viscous fluxes $\mathbf{G}_I^j$ can be evaluated for the use in equation (9), are also obtained in a variational form (Lyra *et al.*, 1995) as

$$\left[\mathbf{M}_\mathrm{L}\frac{\partial \mathbf{U}}{\partial x_j}\right]_I = \sum_{s=1}^{m_I}\frac{C^j_{II_s}}{2}(\mathbf{U}_I + \mathbf{U}_{I_s}) - \left\langle \sum_{f=1}^{2} D_f n_j (5\mathbf{U}_I + \mathbf{U}_{J_f})\right\rangle_I \tag{11}$$

The semi-discrete finite element formulation (equation (9)) represents a central difference type of approximation to the spatial derivatives and can be written in the following form

$$\frac{\mathrm{d}\mathbf{U}}{\mathrm{d}\tau} + \mathbf{I}^M\frac{\mathrm{d}\mathbf{U}}{\mathrm{d}t} = [\mathbf{M}_\mathrm{L}]^{-1}\mathbf{R}, \tag{12}$$

where t and τ in this equation are treated differently.

Real-time discretization

In this work, a dual-time approach is employed for marching equation (12) in time. The real-time t which controls the accuracy of the solution in time is discretized using a second-order implicit backward difference formula. The resulting equation becomes

$$\frac{\mathrm{d}\mathbf{U}^{n+1}}{\mathrm{d}\tau} + \mathbf{I}^M\frac{3\mathbf{U}^{n+1} - 4\mathbf{U}^n + \mathbf{U}^{n-1}}{2\Delta t} = \left[\mathbf{M}_L^{n+1}\right]^{-1}\mathbf{R}^{n+1} \tag{13}$$

where superscript n denotes the current time t, and $n-1$ refers to the previous time-step $t-\Delta t$, while the unknowns are calculated at time $t+\Delta t$ shown by $n+1$. Now equation (13) can be written in a simpler form as

$$\frac{\mathrm{d}\mathbf{U}^{n+1}}{\mathrm{d}\tau} = \tilde{\mathbf{R}}^{n+1} \tag{14}$$

where $\tilde{\mathbf{R}}$ contains the right hand side of equation (13) and the second term on the left hand side of this equation. Equation (14) represents a pseudo-time evolution of flow field and has no physical meaning until the steady-state in pseudo-time is reached. In other words, a divergence-free velocity field is only

obtained when the solution of equation (14) reaches the steady-state. The computational procedure for solving this equation is described below.

Artificial dissipation method

The method used here is a well-known and computationally efficient AD scheme developed by Jameson *et al.* (1981). In this method, a background diffusion term is added to the right hand side of equation (14) to stabilize the numerical scheme and to remove the spurious numerical oscillations. The diffusion $\mathbf{D}_I$ added to a generic node I is constructed as a fourth-order operator in the form of

$$\mathbf{D}_I = -\sum_{s=1}^{m_I} \epsilon_{II_s}^{(4)} (\nabla^2 \mathbf{U}_{I_s} - \nabla^2 \mathbf{U}_I) \frac{\min(\lambda_I, \lambda_{I_s})}{m_I + m_{I_s}}, \tag{15}$$

where the second-order operator is approximated according to

$$\nabla^2 \mathbf{U}_I \approx \frac{1}{m_I} \sum_{s=1}^{m_I} (\mathbf{U}_{I_s} - \mathbf{U}_I) \tag{16}$$

Here m_I denotes the number of edges connected to the node I and λ is the maximum absolute eigenvalue of the Jacobian matrix $l_j \partial \mathbf{F}^j / \partial \mathbf{U}$, where $\mathbf{l} = (l_1, l_2)$ is the unit vector in the direction of the edge II_s. It must be noted that the accuracy of this approximation is degraded when a non-uniform grid is used. Therefore, a mesh with smoothly varying element sizes must be used to achieve an acceptable accuracy. The tuning parameter $\epsilon_{II_s}^{(4)}$ is a constant whose value must be optimized for each problem. A value between 0.01 and 0.05 was found to be appropriate for the problems solved in this paper.

A three-stage Runge-Kutta scheme is employed to advance the solution from pseudo-time level τ^m to $\tau^{m+1} = \tau^m + \Delta\tau$. Within each pseudo-time-step, the solution is advanced according to the following stages

$$\begin{aligned} \mathbf{U}_I^{(0)} &= \mathbf{U}_I^n \\ \mathbf{U}_I^{(k)} &= \mathbf{U}_I^n - \alpha_k \Delta\tau \left(\tilde{\mathbf{R}}_I^{(k-1)} - [\mathbf{M}_L]^{-1} \mathbf{D}_I^{(0)} \right) \text{ for } k = 1, 2, 3 \\ \mathbf{U}_I^{m+1} &= \mathbf{U}_I^{(3)} \end{aligned} \tag{17}$$

Here $\tilde{\mathbf{R}}_I^{(k-1)}$ represents the right hand side of equation (14) computed at the stage $k-1$ for the time level τ^{n+1}, while the added diffusion $\mathbf{D}_I$ is held constant at the value computed at τ^n. The values $\alpha_1 = 0.6$, $\alpha_2 = 0.6$ and $\alpha_3 = 1$ are adopted for the coefficients in equation (17). It must be emphasized that the Runge-Kutta procedure starts at the real-time t^n and only when the steady-state condition is reached in pseudo-time, a divergence-free velocity field is obtained and $\mathbf{U}^{m+1}$ becomes equal to the real-time solution $\mathbf{U}^{n+1}$.

As the accuracy of the pseudo-time marching does not affect the accuracy of the solution in real-time, in this work, a local time-stepping approach (Manzari, 1999) is used to accelerate the convergence rate towards the steady-state in pseudo-time.

The choice of AC parameter

The value of the AC parameter β^2 directly influences the rate of convergence of the solution. Soh and Goodrich (1998) used a one-dimensional inviscid model to obtain a criterion for choosing a suitable value for β^2. This assumption simplifies equation (13) to

$$\frac{\partial}{\partial \tau}\begin{bmatrix} p \\ u \end{bmatrix} + \begin{bmatrix} 0 & \beta^2 \\ \alpha & 2\alpha u \end{bmatrix} \frac{\partial}{\partial x}\begin{bmatrix} p \\ u \end{bmatrix} = \begin{bmatrix} 0 \\ -u + (4u^n - u^{n-1})/3 \end{bmatrix} \tag{18}$$

where $\alpha = 2\Delta t/3$. Note that the pseudo-term has only been added after the real-time discretization. The eigenvalues of equation (18) are $\lambda = \alpha u \pm \sqrt{(\alpha u)^2 + \alpha\beta^2}$. These eigenvalues are real with opposite sign. Therefore, the model behaves as a subsonic compressible flow with an artificial Mach number $M = \alpha u/\sqrt{\alpha\beta^2}$. A good convergence can be achieved by choosing a transonic Mach number such as $1/\sqrt{3}$. This means that a choice of $\beta^2 = 2u^2\Delta t$ should provide a good convergence rate. In multi-dimensional problems, however, the choice of the characteristic velocity which can represent the flow is not always clear. As a general rule, $\sqrt{u_1^2 + u_2^2}$ may be used in such cases.

In practice, the size of Δt might be chosen to be very small to resolve the significant features of the flow field. This will consequently result in a very small value for the AC parameter which cause negative effect on the convergence rate of the solution in pseudo-time. It is found that $\beta^2 = 1$ provides a good lower limit for the AC parameter when the above criteria is used.

Test cases

In this section, the accuracy and performance of the proposed method is demonstrated by solving a number of test cases including both external and internal flows. The first two test cases are external flow problems with different characteristics. One of these is a simple transient problem with an ultimate steady-state solution while the other is a von Kármán vortex street flow which exhibits a periodic behavior. The second set of test cases studies the flow inside a closed cavity. Again, one test case solves an impulsive start of the lid and the second case simulates the solution when the lid has a reciprocative movement.

The largest time-step Δt is chosen such that it can reveal the important features of the flow. For some cases, the results are also obtained using smaller

time-steps to show the convergence trend. The pseudo-time-step $\Delta\tau$ is chosen between $\Delta t/50$ and $\Delta t/20$. Depending on the problem a total number of pseudo-time sub-iterations between 200 and 1,000 was found to be enough to reach a converged solution in pseudo-time.

Impulsively started cylinder

This test case demonstrates the growth of a separation bubble in the wake region of a circular cylinder in a flow with $\mathrm{Re} = 40$. The problem has been extensively studied using both experiments (Coutanceau and Bouard, 1976) and numerical simulations (Braza *et al.*, 2000; Collins and Dennis, 1973; Gaitonde, 1998). In this problem, a cylinder of diameter $d = 1$ is placed at the center of an outer circular boundary of diameter $D = 50$. A free-stream boundary condition is imposed at the outer boundary. The computational grid used here is a 161×101 O-grid as shown in Figure 1 in which the circumference of the cylinder is divided into 161 uniformly spaced nodes. The height of the first grid layer adjacent to the cylinder is 0.02 and increases gradually towards the outer boundary. The problem was solved using $\Delta t = 0.1$ and a total of 200 pseudo-time iterations were allowed within each real-time-step which normally resulted in three order of magnitude drop in the L^2-norm of the pressure residual.

The growth of the length of the separation bubble or the re-attachment length L_s with time is shown in Figure 1. This length represents the position of the point where the flow velocity changes sign along the centerline. It is seen that the prediction obtained by the current method is in good agreement with those reported by Collins and Dennis (1973) and Coutanceau and Bouard (1976). Figure 2 shows the variation of the streamlines during the transition to its steady-state.

Vortex shedding

The second test case studies the so-called von Kármán vortex street problem for two Reynolds numbers 200 and 1,000. There are several experimental (Tokumaru and Dimotakis, 1991; Williamson, 1989) and computational (Balir *et al.*, 1990; Braza *et al.*, 2000; He *et al.*, 2000) work investigating various aspects of this interesting and practically important flow.

The computational domain is a rectangle $(-15, 45) \times (-15, 15)$ wherein a circular cylinder of diameter $d = 1.0$ placed at (0, 0). The flow is from the left to the right and the boundaries are considered as far-field with a free-stream boundary condition. The computational grid used for this test case is shown in Figure 3. This grid consists of 7,639 triangular elements and 3,889 nodes.

The initial condition for this problem is a uniform flow. Figures 4 and 5 show the variations of the lift coefficient with time for $\mathrm{Re} = 200$ and 1,000, respectively. The results given in He *et al.* (2000) are also shown for

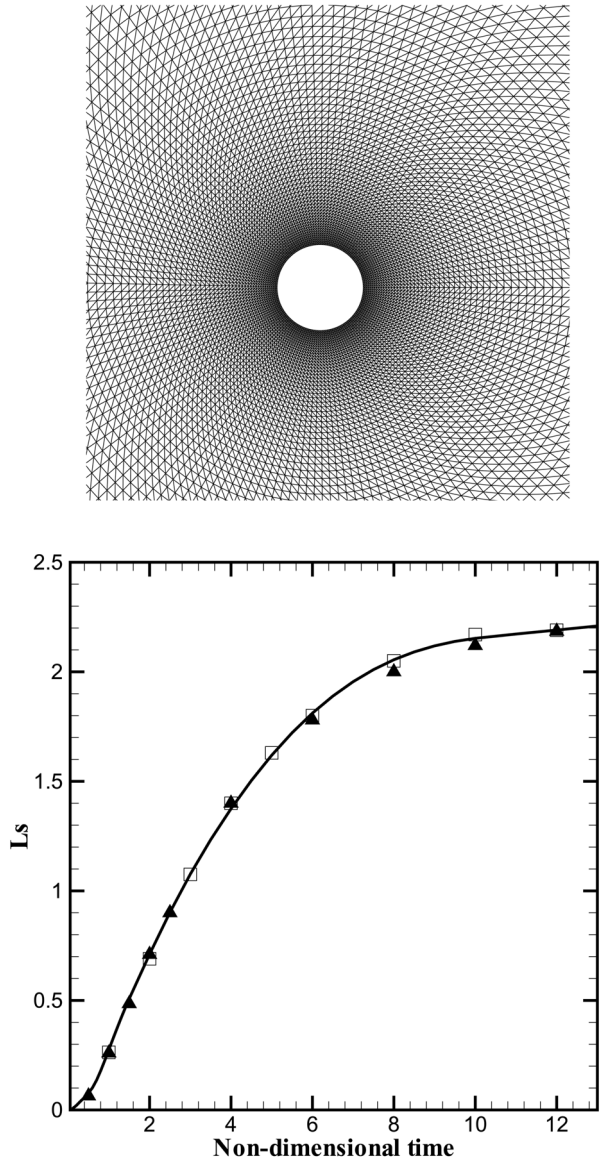

Figure 1.
Impulsively started cylinder, computational grid (top) and variation of the re-attachment length with time (bottom)- Line, present method; square: Coutanceau and Bouard; triangle: Collins and Dennis

comparison. The amplitude and period of the results are in good agreement with those presented by He *et al.* (2000). The Strouhal number $S_n = \mathrm{d}f_n/U_\infty$ (f_n is the frequency) calculated for $\mathrm{Re} = 200$ and 1,000 are 0.20 and 0.238, respectively. Figures 6 and 7 show the time evolution of the streamlines corresponding to $\mathrm{Re} = 200$ and 1,000, respectively. These figures visualize how alternating vortices are formed, advected and diffused downstream.

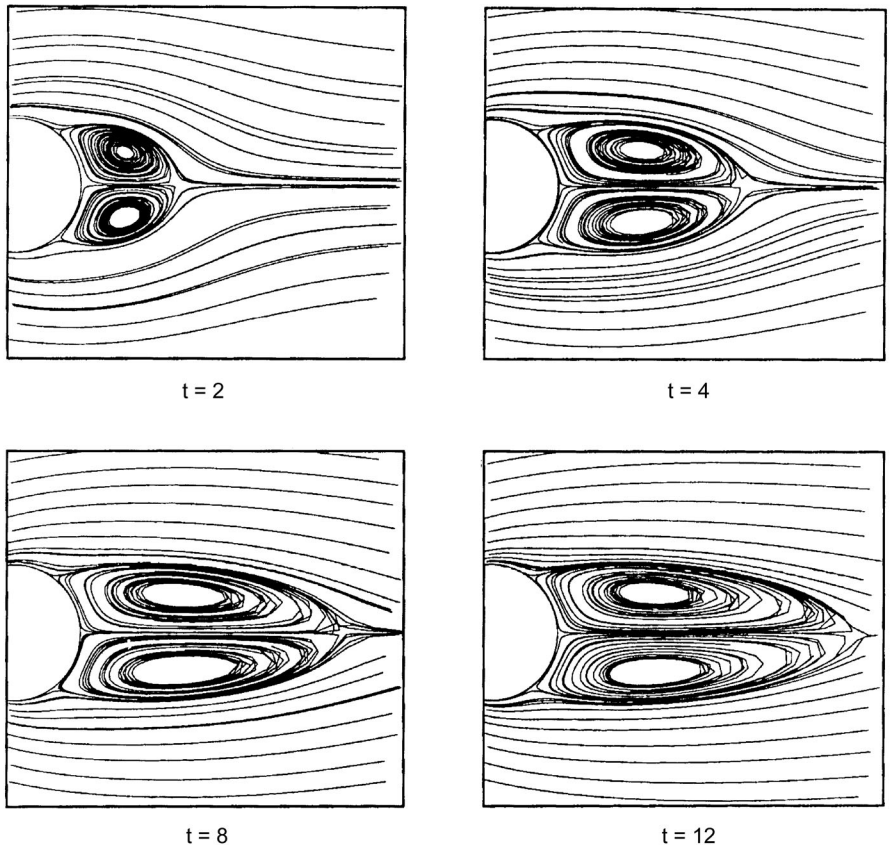

Figure 2.
Impulsively started cylinder: wake development

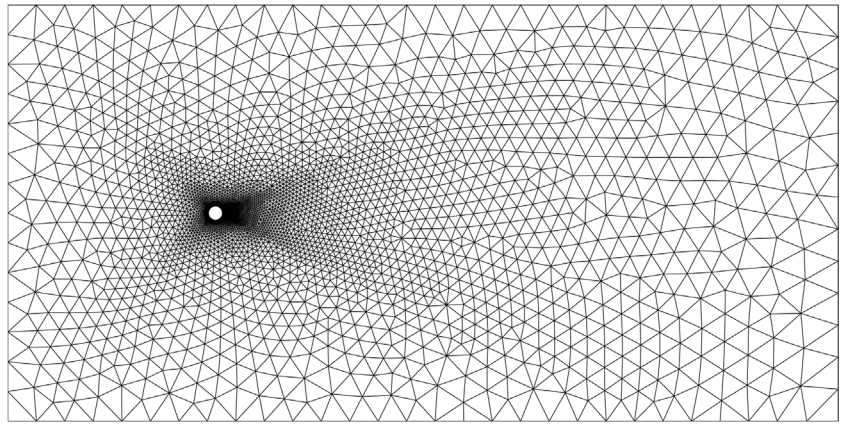

Figure 3.
von Kármán vortex street: computational grid

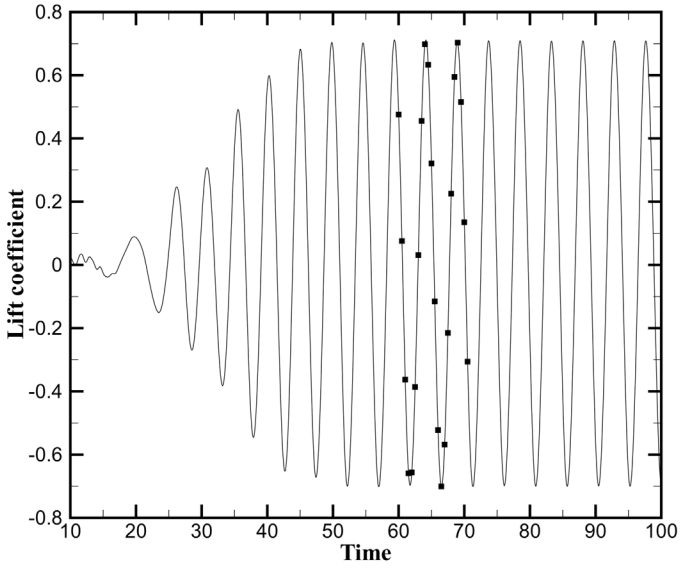

Figure 4.
von Kármán vortex street: variation of lift coefficient for Re = 200; line: Computed, symbols: He *et al.* (2000)

Lid-driven cavity flow

The first internal flow test case involves flow inside a square cavity (1×1) that its upper wall (lid) moves with a certain velocity. For $t < 0$, the lid has zero velocity but for $t \geq 0$ it suddenly reaches a speed of $u = 1$. The development of the flow field during this impulsive start is of main concern here. The problem is solved for two different Reynolds numbers, Re = 100 and 400.

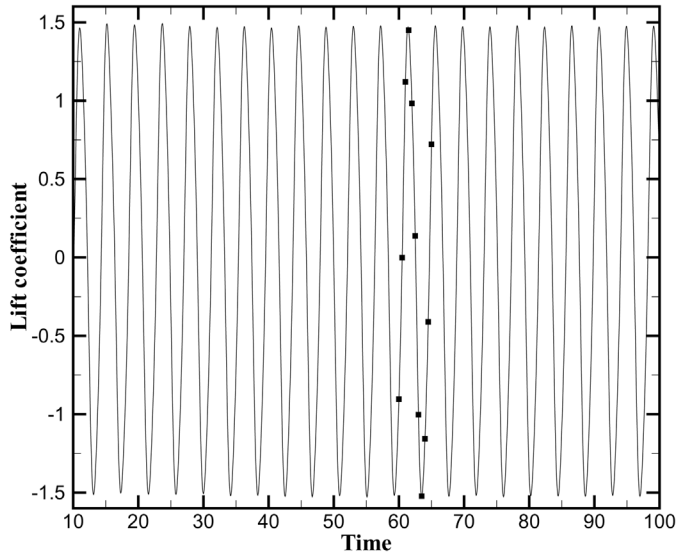

Figure 5.
von Kármán vortex street: variation of lift coefficient for Re = 1,000; Line: Computed, symbols: He *et al.* (2000)

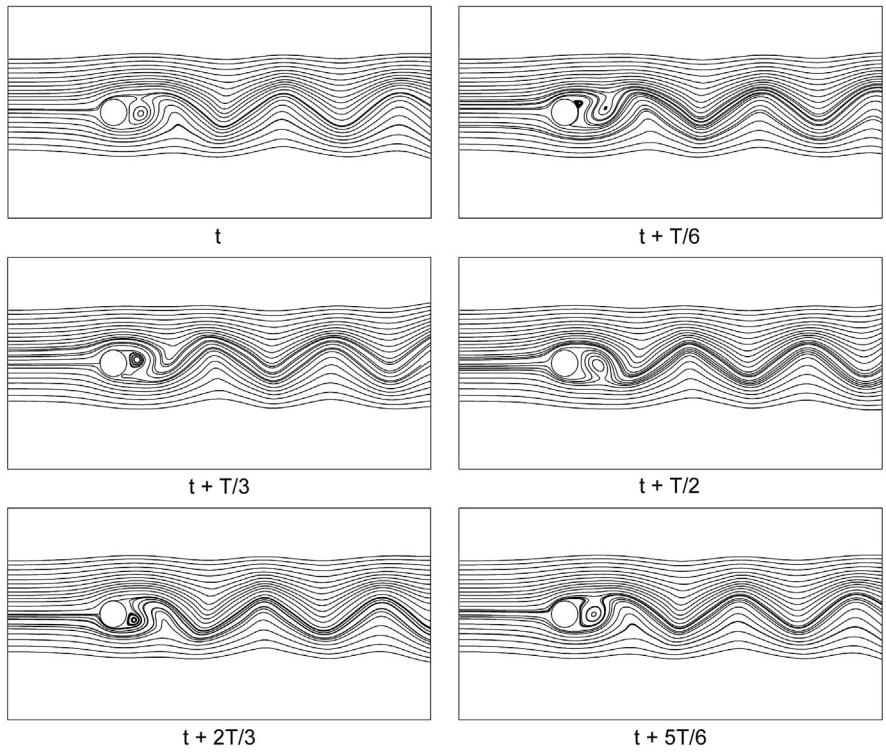

Figure 6.
von Kármán vortex street: streamlines within a period T for $\mathrm{Re} = 200$

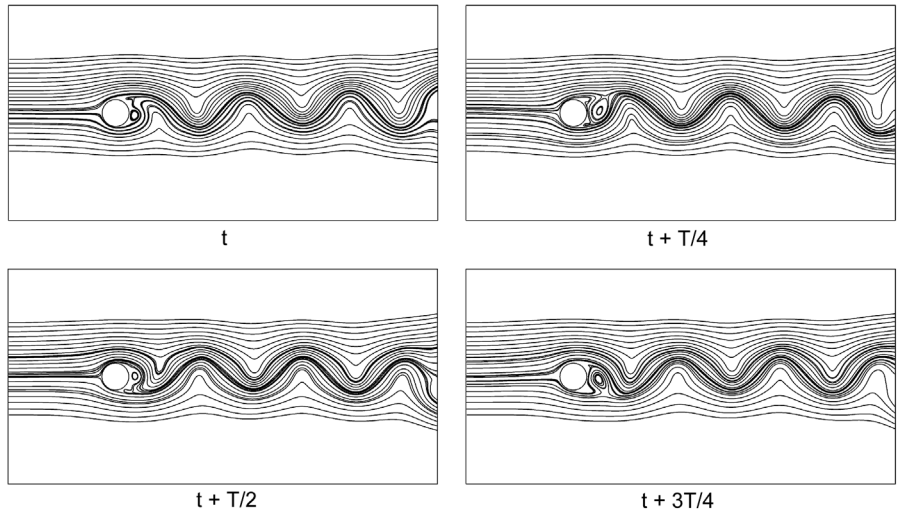

Figure 7.
von Kármán vortex street: streamlines within a period T for $\mathrm{Re} = 1,000$

The computational grid (Figure 8) used for this case consists of 51×51 nodes and 5,000 triangular elements. On the bottom wall and the side walls a no-slip boundary condition is imposed. Figure 9 shows the variation of the horizontal velocity at the center of the cavity. The computed results are in close agreement with those presented by Dailey and Pletcher (1996). Here, two time-steps ($\Delta t = 0.125$ and 0.0125) were used. As can be seen from Figure 9, this refinement has not had significant effect on the result for $\mathrm{Re} = 100$ as reported in Daily and Pletcher (1996). However, in the case of $\mathrm{Re} = 400$, slightly lower minimum values was predicted when $\Delta t = 0.0125$ was used. The final steady-state values are in close agreement with the data presented by Ghia *et al.* (1982).

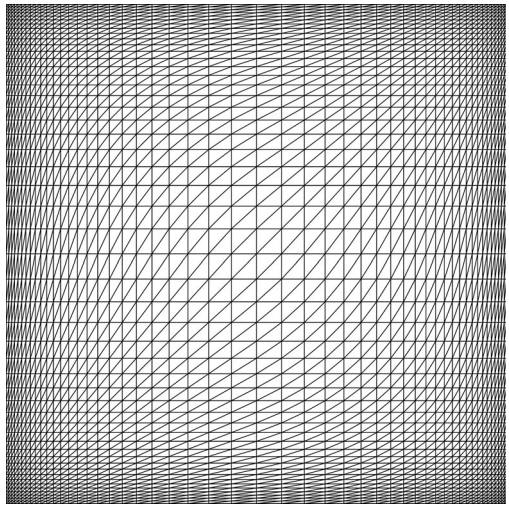

Figure 8.
Lid driven cavity: computational grid

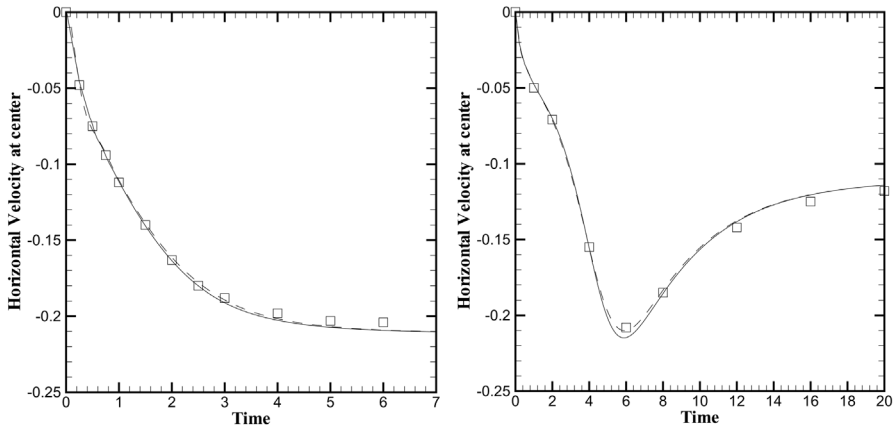

Figure 9.
Lid driven cavity: variation of the horizontal velocity at center with time for $\mathrm{Re} = 100$ (left) and $\mathrm{Re} = 400$ (right); solid line: present method with $\Delta t = 0.0125$, dashed line: present method with $\Delta t = 0.125$, symbols: Dailey and Pletcher (1996)

Figure 10 shows the development of the velocity field within the cavity at three different stages during the transition to the steady-state for both Re = 100 and 400.

Oscillatory cavity flow

The last test case simulates the flow in the same cavity as previous test case, however, here the lid has an oscillating velocity $u = \cos t$. The period of the oscillations is $T = 2\Pi$. This test case has been studied by Soh and Goodrich (1988) and Gaitonde (1998) for Re = 400. The same computational grid as the previous test case was used for this problem. The time-step was taken to be $\Delta t = T/40$. Figure 11 shows the streamlines at various stages of a complete period. It is noticed that a symmetric pattern is formed after each half period. It is also seen that as time goes different circulation zones are created, move inside the domain and finally collapse. Figure 12 shows the variation of the non-dimensional drag force defined as

$$D = \int_0^1 \left(\frac{\partial u}{\partial y}\right)_{y=1} \mathrm{d}x$$

with time. The results are in good agreement with the data given by Soh and Goodrich (1988).

Conclusions

A combination of the AC model and an AD algorithm was used in a dual-time context to solve the incompressible Navier-Stokes equations. The method has been successfully tested against several internal and external transient incompressible fluid flow problems. In all these cases, no convergence problem was experienced and normally three orders of magnitude drop in the L_2-norm of the residuals of the primitive variables was achieved within a small number of iterations. The use of a second-order backward difference formula for the real-time discretization proved to be effective and yet inexpensive. Also, the use of a lumped mass matrix in the finite element implementation has shown no negative effect for the range of problems solved here. A study of the effect of the artificial compressibility parameter revealed that although a theoretical optimum value can be found for this parameter, in certain problems, this is too limiting and a value of order unity can be normally used without any compromise. The overall structure of the solution procedure remains the same as its compressible flow counterpart which has shown good scalability on various parallel computing platforms. Therefore, the current scheme can be easily adopted in a parallel environment producing virtually the same speed-up factor. The proposed scheme is currently extended to free surface flows where a time-accurate solution plays a crucial role.

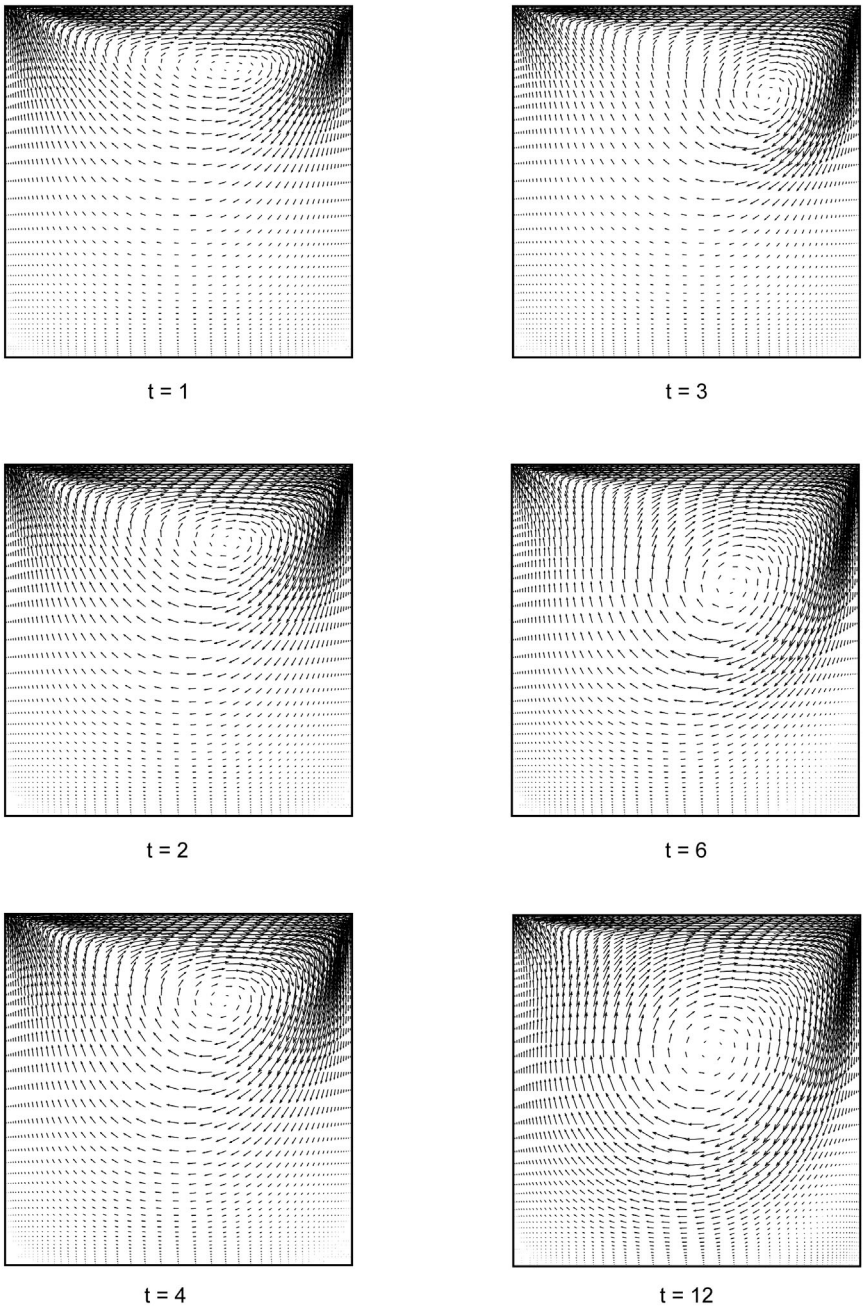

Figure 10.
Lid driven cavity: velocity fields for Re = 100 (left) and for Re = 400 (right)

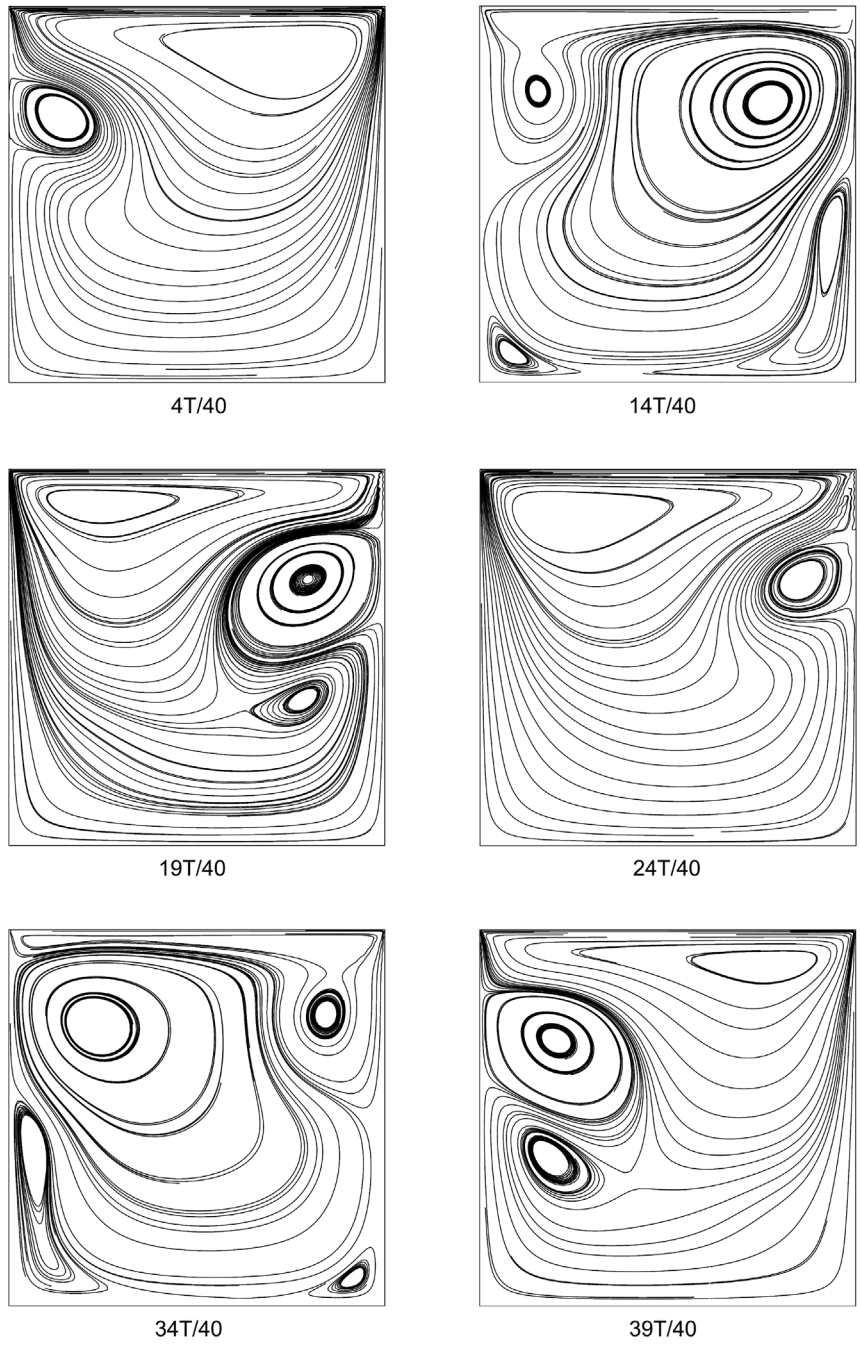

Figure 11.
Oscillating lid driven cavity: streamlines at various times

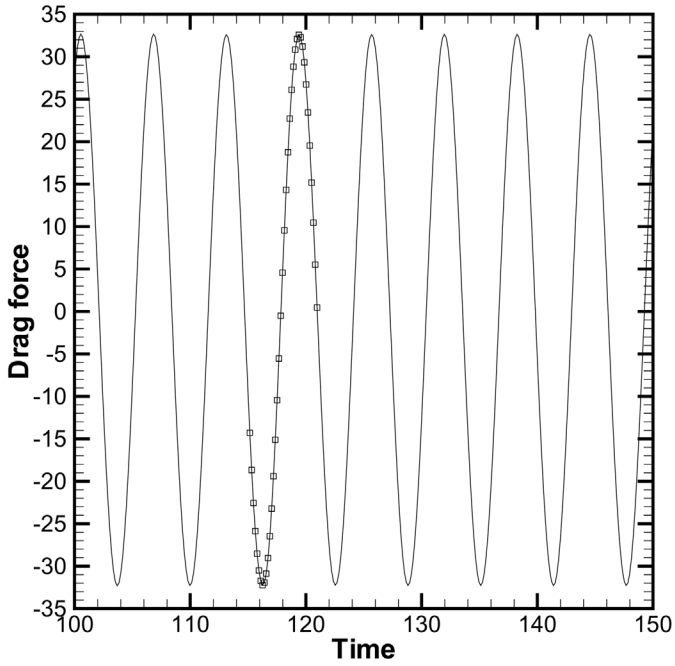

Figure 12.
Oscillating lid driven cavity: variation of non-dimensional drag force with time; Line: present method, symbols: Soh and Goodrich (1988)

References

Badr, H.M., Coutanceau, M., Dennis, S.C.R. and Ménard, C. (1990), "Unsteady flow past a rotating circular cylinder at Reynolds numbers 10^3 and 10^4", *J. Fluid Mech.*, Vol. 220, pp. 459-84.

Braza, M., Chassaing, P. and Ha Minh, H. (2000), "Numerical study and physical analysis of the pressure and velocity fields in the near wake of a circular cylinder", *J. Fluid Mech.*, Vol. 165, pp. 79-130.

Brooks, A.N. and Hughes, T.J.R. (1982), "Streamline upwind/Petrov-Galerkin formulation for convection dominated flows with particular emphasis on the incompressible Navier-Stokes equations", *Comp. Methods Appl. Mech. Eng.*, Vol. 32, pp. 199-259.

Chorin, A.J. (1967), "A numerical method for solving incompressible viscous flow problems", *J. Comp. Physics*, Vol. 2, pp. 12-26.

Collins, W.M. and Dennis, S.C.R. (1973), "Flow past an impulsively started cylinder", *J. Fluid Mech.*, Vol. 60, pp. 105-27.

Coutanceau, M. and Bouard, R. (1976), "Experimental determination of the main features of the viscous flow in the wake of a circular cylinder", *J. Fluid Mech.*, Vol. 79, pp. 257-72.

Dailey, L. and Pletcher, R.H. (1996), "Evaluation of multigrid acceleration for preconditioned time-accurate Navier-Stokes algorithms", *Computers Fluids*, Vol. 25 No. 8, pp. 791-811.

Gaitonde, A. (1998), "A dual-time method for two-dimensional unsteady incompressible flow calculations", *Int. J. Numer. Methods Eng.*, Vol. 41, pp. 1153-66.

Gatiganti, R.M., Badcock, K.J., Cantariti, F., Dubuc, L., Woodgate, M. and Richards, B.E. (1998), "Evaluation of an unfactored method for the solution of the incompressible flow equations using artificial compressibility", *Applied Ocean Research*, Vol. 20, pp. 179-87.

Ghia, U., Ghia, K.N. and Shin, C.T. (1982), "High-Re solutions for incompressible flow using the Navier-Stokes equations and a multigrid method", *J. Comp. Phys.*, Vol. 48, pp. 387-411.

Gresho, P.M. and Sani, R.L. (2000), *Incompressible Flow and the Finite Element Method*, Wiley, Chichester, England, Vols. 1 and 2.

He, J.W., Glowinski, R., Metcalfe, R., Nordlander, A. and Periaux, J. (2000), "Active control and drag optimization for flow past a circular cylinder", *J. Comp. Phys.*, Vol. 163.

Jameson, A., Schmidt, W. and Turkel, E. (1981), "Numerical simulation of the Euler equations by the finite volume method using Runge-Kutta time stepping schemes", *AIAA Paper*, 81-1259.

Lewis, R.W. and Ravindran, K. (2000), "Finite element simulation of metal casting", *Int. J. Numer. Methods Eng.*, Vol. 47, pp. 29-59.

Lyra, P.R.M., Manzari, M.T., Morgan, K., Hassan, O. and Peraire, J. (1995), "Upwind side-based unstructured grid algorithms for compressible viscous flow computations", *Int. J. Eng. Anal. Des.*, Vol. 2, pp. 197-211.

Manzari, M.T. (1999), "An explicit finite element algorithm for convection heat transfer problems", *International Journal of Numerical Methods in Heat and Fluid Flow*, Vol. 9 No. 8, pp. 860-77.

Manzari, M.T., Hassan, O., Morgan, K. and Weatherill, N.P. (1998), "Turbulent flow computations on 3D unstructured grids", *Finite Elements in Analysis and Design*, Vol. 30, pp. 353-63.

Massarotti, N., Nithiarasu, P. and Zienkiewicz, O.C. (1998), "Characteristic-based-split (CBS) algorithm for incompressible flow problems with heat transfer", *International Journal of Numerical Methods in Heat and Fluid Flow*, Vol. 8 No. 8, pp. 969-90.

Merkle, C.L. and Athavale, M. (1987), "Time-accurate unsteady incompressible flow algorithm based on artificial compressibility", *AIAA Paper*, pp. 87-1137.

Morgan, K. and Peraire, J. (1998), "Unstructured grid finite-element methods for fluid mechanics", *Reports on Progress in Physics*, Vol. 61, pp. 569-638.

Peraire, J., Morgan, K. and Peiró, J. (1994), "The simulation of 3D incompressible flows using unstructured grids", in Coughey, D.A. and Hafez, M. (Eds), *Frontiers of Computational Fluid Dynamics*, Wiley, New York, pp. 281-301.

Peraire, J., Peiró, J. and Morgan, K. (1993), "Multigrid solution of the 3-D compressible Euler equations on unstructured tetrahedral grids", *Int. J. Numer. Methods Eng.*, Vol. 36 No. 6, pp. 1029-44.

Rogers, E. and Kwak, D. (1989), "Numerical solution of the incompressible Navier-Stokes equations for steady and time-dependent problems", *AIAA Paper*, pp. 89-1463.

Soh, W.Y. and Goodrich, J.W. (1988), "Unsteady solution of incompressible Navier-Stokes equations", *J. Comp. Phys.*, Vol. 79, pp. 113-34.

Tokumaru, P.T. and Dimotakis, P.E. (1991), "Rotary oscillation control of a cylinder wake", *J. Fluid Mech.*, Vol. 224, pp. 77-90.

Wasfy, T., West, A.C. and Modi, V. (1998), "Parallel finite element computation of unsteady incompressible flows", *Int. J. Numer. Methods Fluids*, Vol. 26, pp. 17-37.

Williamson, C.H.K. (1989), "Oblique and parallel modes of vortex shedding in the wake of a circular cylinder at low Reynolds numbers", *J. Fluid Mech.*, Vol. 206, pp. 579-628.

Further reading

Ingham, D.B. and Tang, T. (1990), "A numerical investigation into the steady flow past a rotating circular cylinder at low and intermediate Reynolds numbers", *J. Comp. Phys.*, Vol. 87, pp. 91-107.

Lin, F.B. and Sotiropoulos, F. (1997), "Assessment of artificial dissipation models for three-dimensional incompressible flow solutions", *J. Fluids Eng. – Trans. ASME*, Vol. 119 No. 2, pp. 331-40.